Determinants of heart rate in Svalbard reindeer reveal mechanisms of seasonal energy management

Electronic Supplementary Material (ESM)

L. Monica Trondrud*, Gabriel Pigeon, Steve Albon, Walter Arnold, Alina L. Evans, R. Justin Irvine, Elżbieta Król, Erik Ropstad, Audun Stien, Vebjørn Veiberg, John R. Speakman, Leif Egil Loe
*Corresponding author: monica.trondrud@gmail.com; monica.trondrud@nmbu.no

Contents

Appendix 1: Additional methods

1.a Study system

The study area includes Colesdalen and Northern Reindalen with adjacent side valleys on the Nordenskiöld peninsula (Figure S1) on the western part of Spitsbergen, Svalbard. This part of Svalbard receives mild ocean currents from the south and sea ice forms relatively late in the year compared to the east coast of Svalbard [1]. The area is characterized by wide, U-shaped valleys which are mostly vegetated up to about 250 meters above sea level. Ridge communities on the upper part of the hillsides are characterized by the presence of the dwarf shrubs *Dryas octopetala* and *Salix polaris*, and on the shallow slopes graminoid vegetation can be found in patches [1]. Heathlands, together with moist moss vegetation and wetlands, are typical characteristics of the lower-lying parts of the valleys [1]. Although live vascular plant biomass in vegetated habitats averages 35 g m^{-2} (annual range 23–46 g m^{-2} [2]), the area supports a high density of reindeer compared to other parts of Svalbard [3]. In summer, reindeer forage mostly in lower-lying, wetter and more productive pastures. In winter, snow and ice normally limit the access to these areas, and reindeer tend to feed on wind-blown, vegetated ridges, where the quality and energy content of forage is poorer than in summer [1,4].

Figure S1. Map of the study area (red lines) on Nordenskiöld Land. The inset shows Nordenskiöld Lands position on Spitsbergen, the largest island on the Svalbard archipelago. ©Norwegian polar institute (https://toposvalbard.npolar.no/).

1.b Surgical procedure for biologger deployment and retrieval

All implants were sterilized with ethylene oxide gas (Anaprolene AN74i 60 L, Andersen Europe, Kortrijk, Belgium). Prior to biologger implantation, the animals were sedated with intranasal medetomidine (Domitor vet, Orion Pharma Animal Health, Finland; dose ~0.14 mg kg^{-1} body mass, BM) or dexmedetomidine (Dexdomitor vet, Orion Pharma Animal Health, Finland, dose ~0.07 mg kg^{-1} BM). For local anaesthesia, we used 2.5–5 mg of Bupivacaine (Marcaine 5 mg mL^{-1}, AstraZeneca, Cambridge, UK). Post-operative analgesia (0.5 mg kg^{-1} meloxicam; Metacam®, Boehringer Ingelheim Vetmedica GmBH, Germany) was administered subcutaneously prior to surgery. Surgical anaesthesia was assessed by checking the eyelid reflexes, limb movements, pulse and breathing rate. The surgical area was shaved and cleaned with chlorhexidine spirit. The logger was inserted into the subcutaneous space through a ~1 cm incision, which was then closed with 2-0 monofilament absorbable suture PDS® II (polydioxanone) (Ethicon, Johnson & Johnson, New Brunswick, NJ, United States). After surgery was completed, anaesthesia was reversed with intramuscular atipamezole (Antisedan® 5 mg mL^{-1}, Orion Pharma Animal Health, Turku, Finland; 5 mg mg^{-1} medetomidine or 10 mg mg^{-1} dexmedetomidine). Once animals regained consciousness and coordination, they were released and monitored until walking/running with normal balance (typically ~5 min post-injection of the antidote). Normal balance was considered as walking/running in straight lines and not stumbling when standing upright or walking.

When retrieving the loggers in 2019, animals were manually restrained and local anaesthesia was used (2.5–5 mg of Bupivacaine; Marcaine 5 mg mL^{-1}, AstraZeneca, Cambridge, UK) together with post-operative analgesia (0.5 mg kg^{-1} meloxicam; Metacam®, Boehringer Ingelheim Vetmedica GmBH, Germany). A small incision (~0.5 cm) was made at the top of the logger through which the logger was pushed out. The incision was left to heal without suture given its small size. The procedure took ~5 min.

1.c Validation and filtering of heart rate data

The DST centi-HRT (Star-Oddi, Gardabaer, Iceland; ~19 g) is a programmable heart rate- and temperature logger [5]. It is a leadless cylindrical device with a ceramic housing (Alumina) with the dimensions (diameter x length): 15 mm x 46 mm. Heart rate was automatically calculated from a 4-sec electrocardiogram (ECG) at 150 Hz measurement frequency and stored alongside a quality index of signal clarity in a non-volatile memory. Each logger can store up to 233,017 measurements per sensor, however several loggers experienced battery failure before maximum capacity was reached (noted in methods in main manuscript). We also programmed the loggers to save a raw ECG signal every 6 hrs alongside the calculated heart rate and quality index. This allowed us to manually validate the accuracy of the internal algorithms. To do so, we plotted the 4-sec ECG signal with a grid background divided into small squares (x), and counting the number of squares between two R waves (Figure S2). We calculated the number of beats per minute from this value (x) using the formula: $HR = \frac{60}{\left(\frac{x \times 4}{15}\right)}$ to derive the value in beats per minute. We calculated the percent deviation of the validated and the calculated heart rate, with the assumption that the validated heart rate was always correct. We considered the reading to be successful if the difference between the two values was less than 10%. From the validations, we asserted that only recordings with quality level 0 were reliable, with a success rate of 94% versus 67%, 31% and 9% for the quality levels 1, 2 and 3, respectively., we found that the reliability of the calculated heart rate decreased substantially at values above 175 bpm, even at quality level 0 (Figure S3), typically caused by “double counting”, where the R and T waves of the same ECG complex are counted as two separate complexes (Figure S4). In future studies, this can be avoided by increasing the minimum time gap between two counts (typically while programming the logger). We therefore filtered heart rate at 175 and 20 bpm. Removing these values in (and retaining only quality level 0) made little change to the results; while the range

of heart rate records was reduced from 16–429 to 20–173 in the winter data and from 20–347 to 20–173 in the summer data, mean values changed only slightly: 39.2 ± 23.4 (pre-filtering) vs 37.2 ± 12.8 (post-filtering) in winter and 100.5 ± 21.3 (pre-filtering) vs 99.7 ± 12.1 (post-filtering) in summer. Furthermore, when comparing filtered validated heart rate and the recorded heart rate in the logger, 94% of the recordings deviated by less than ±5% from the validated heart rate and 98.5% less than ±10% from the validated heart rate. The percentage difference was normally distributed with a mean and standard deviation of 2.5 ± 6.1 %, and a median of 0.1% (figure S5). This potential error may contribute to a minor increase in unexplained variation in our results but is not likely to cause any bias in parameter estimates.

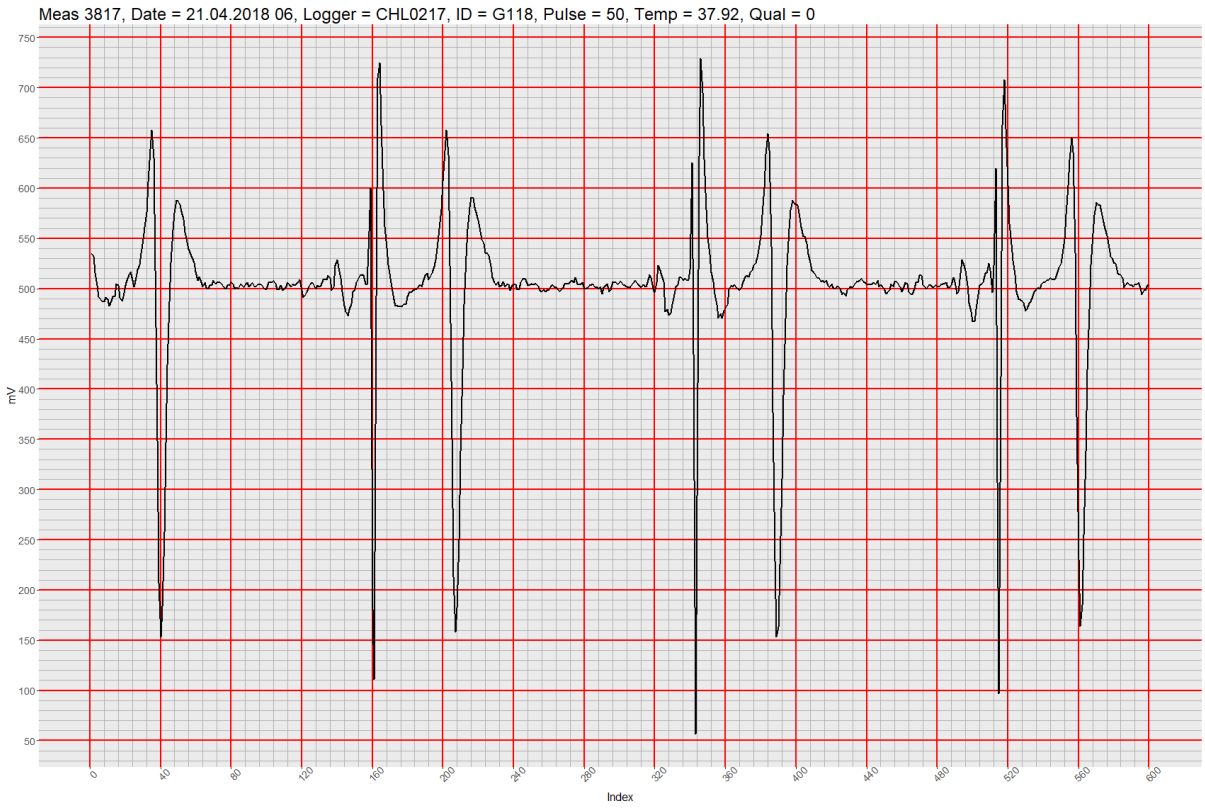

Figure S2. Example of a good quality (quality level 0) ECG signal with correct estimation by the internal algorithm (50 bpm) and the manual validation (4.5 red squares between two QRS complexes = 50 bpm).

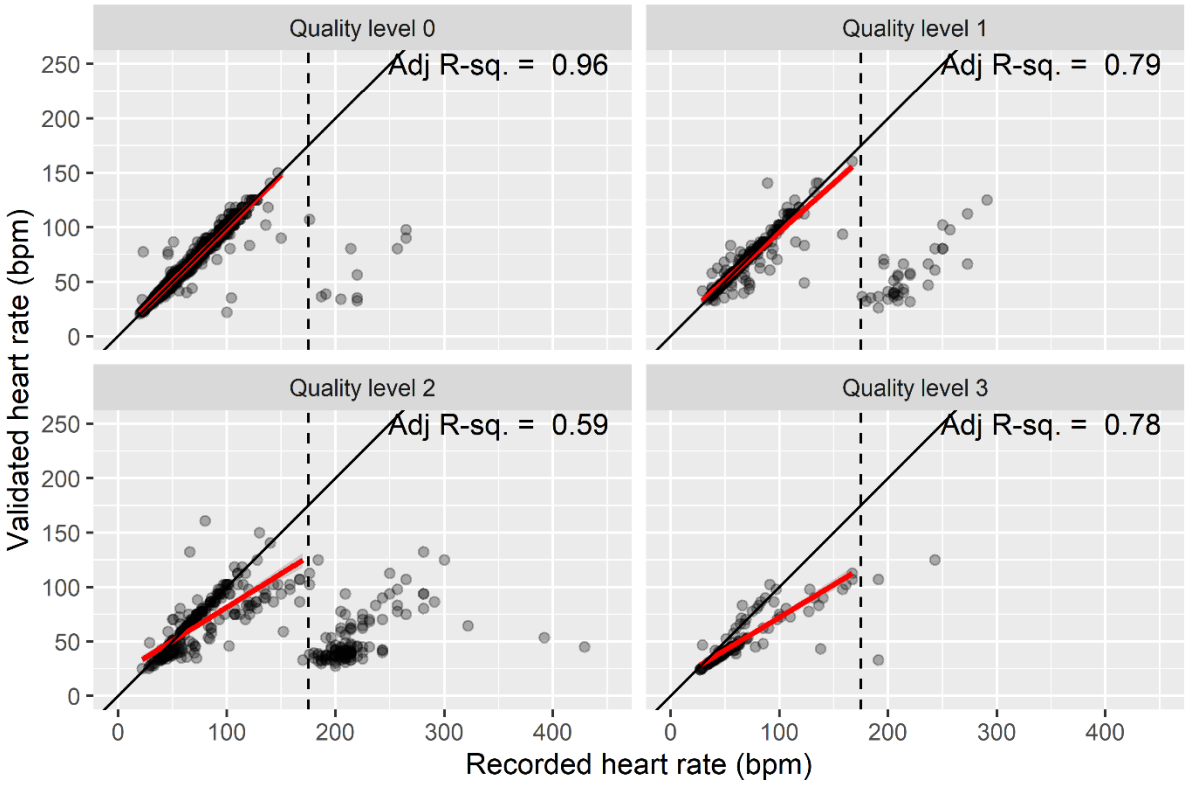

Figure S3. Correlation between recorded heart rate by the DST Centi-HRT loggers (x-axis) and manually validated heart rates from raw ECG signals (y-axis), grouped by quality level. In all quality levels, the difference between recorded and validated heart rate increased drastically for recorded values above 175 bpm (marked with a dashed line). The red lines represent the true correlation between the recorded and validated heart rates, with adjusted R-squared values presented in the panels for each quality level.

Figure S4. Example of an ECG signal (quality level 2) with incorrect estimation by the internal algorithm (225 bpm) and the manual validation (6.6 red squares between two R-waves = 34 bpm), typically resulting from double counts of one ECG cycle.

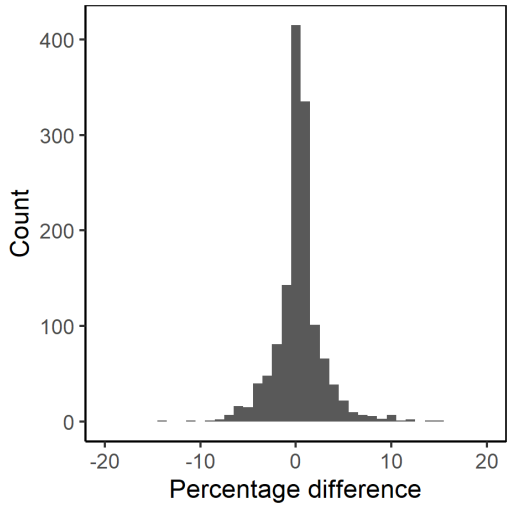

Figure S5. Distribution of the percentage difference between heart rates validated from an ECG signal and heart rates recorded by the logger, after filtering for quality level 0 and minimum and maximum values (>20 and <175 bpm).

1.d Activity data collection and processing

Most of the activity loggers were aligned with round 5-min intervals (16:05, 16:10, etc), but a few were not (e.g. recording at 16:03, 16:08). In the latter cases, the timestamp was rounded to the nearest 5-min timestamp. There was a strong correlation between activity recorded in each axis (X – forward/backward, Y – left/right; Figure S6). In both July and January, the total activity (X+Y) was bimodally distributed with a high frequency of low values (< 50) and a normal distribution of values between 50 and 510 (Figure S7). Acceleration data has not been validated with behavioural observations in Svalbard reindeer, so we could not distinguish activity types (walking, grazing, etc) except resting/stationary (hereafter "resting") and moving (hereafter "active"). We used the threshold of 50 (X + Y) to determine whether animals were resting/stationary based on observations of wild Norwegian reindeer (*R. t. tarandus*), where values below 25 in each axis (X and Y separately) were associated with "resting" and "standing still", whereas any form of non-stationary activity was characterized by higher values above 25 in either direction [7]. In Svalbard reindeer, the activity category "standing" only comprises 0.6% and 6.2% of Svalbard reindeer's time budget during summer and winter, respectively [8]

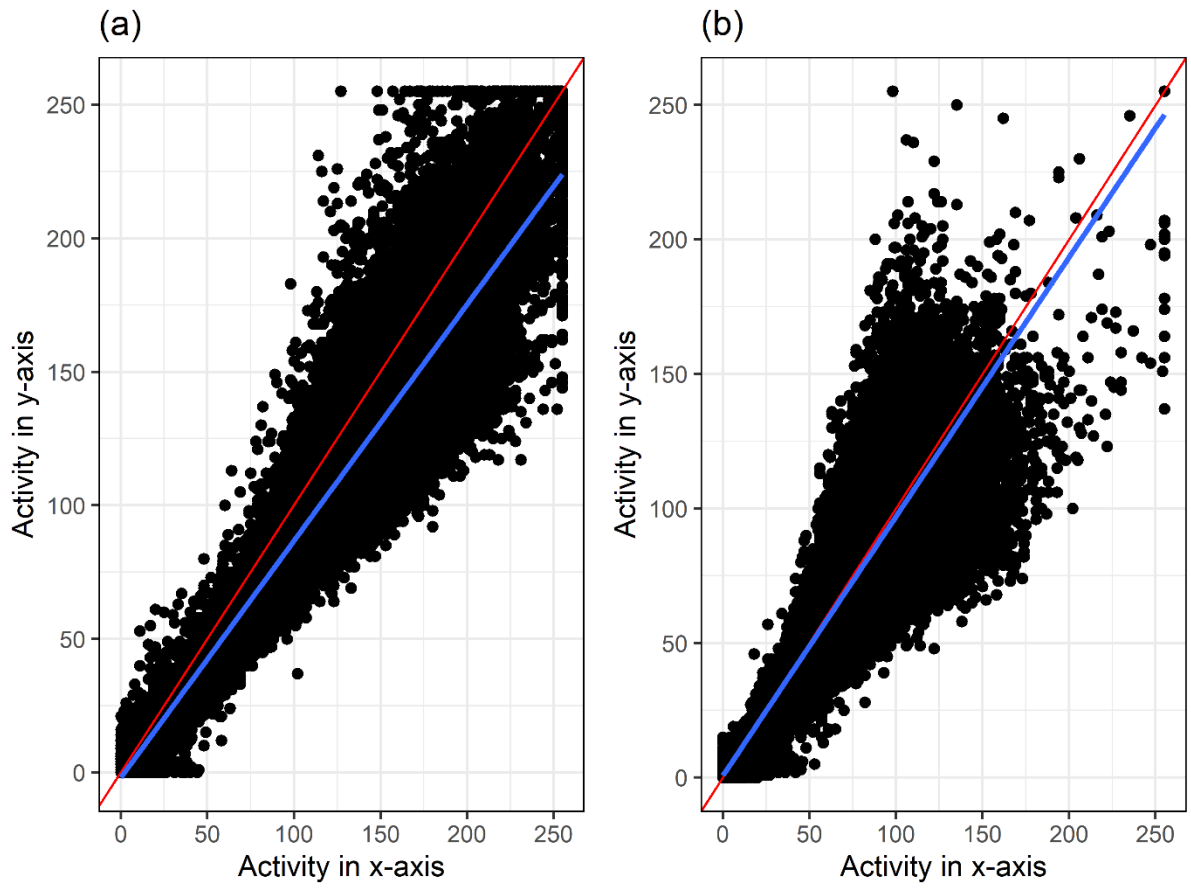

Figure S6. Relationship between activity recordings in the x-axis (back-forward movement) and the y-axis (right-left movement) (a) in summer and (b) winter. The red lines indicate a slope of 1 and intercept of 0, while the blue lines indicate the actual slopes for each season.

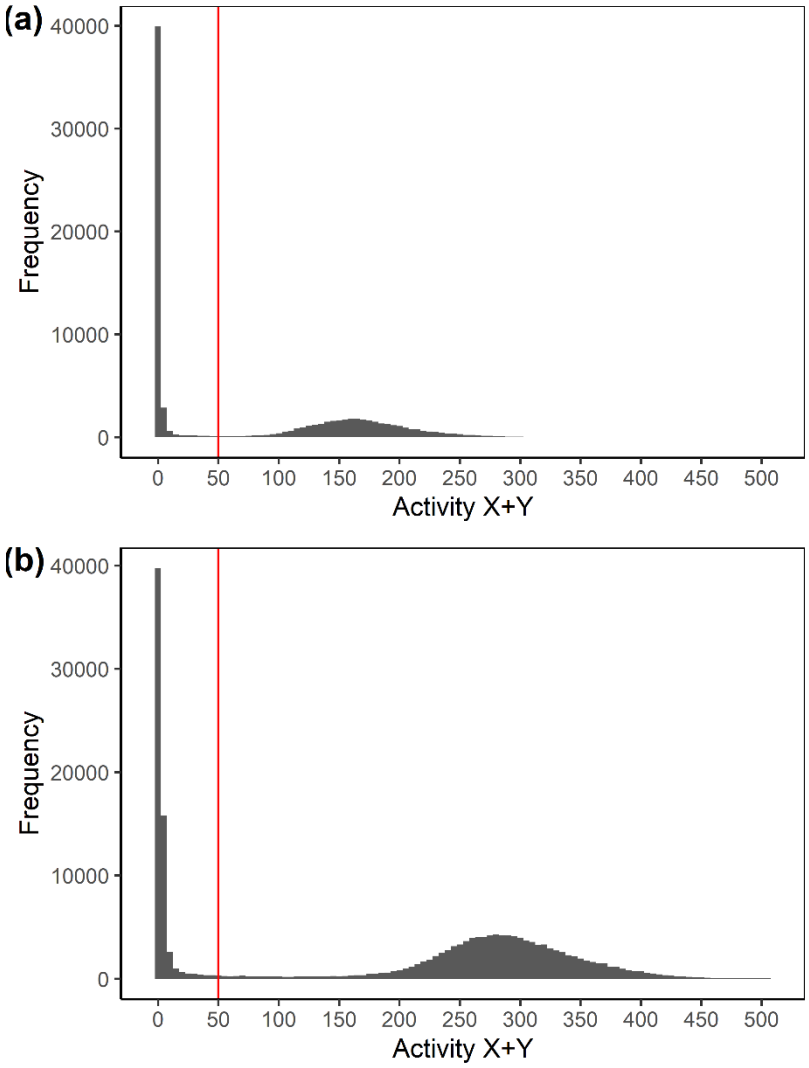

Figure S7. Distribution of all activity recordings (as the sum of activty in X- and Y-axes collected every 5 min) in (a) winter and (b) summer. The vertical red line indicates the treshold (value of 50) that was used to separate “resting” and “active” states.

1.e Temperature data collection and comparisons

The black bulb thermistor was constructed using a copper bulb of 15 cm in diameter painted black (figure S8a). Placed in the center of the bulb was a single Thermocron iButton temperature sensor (model no. DS1922L; iButtonLink, Whitewater, Wisconsin, US) which has a temperature range of –40°C to +85°C with a software corrected accuracy of ± 0.5°C in the range of –10°C to +65°C. The sensor was programmed to record temperature every 4 hrs and was situated centrally in Colesdalen (Figure S1, Figure S8b).

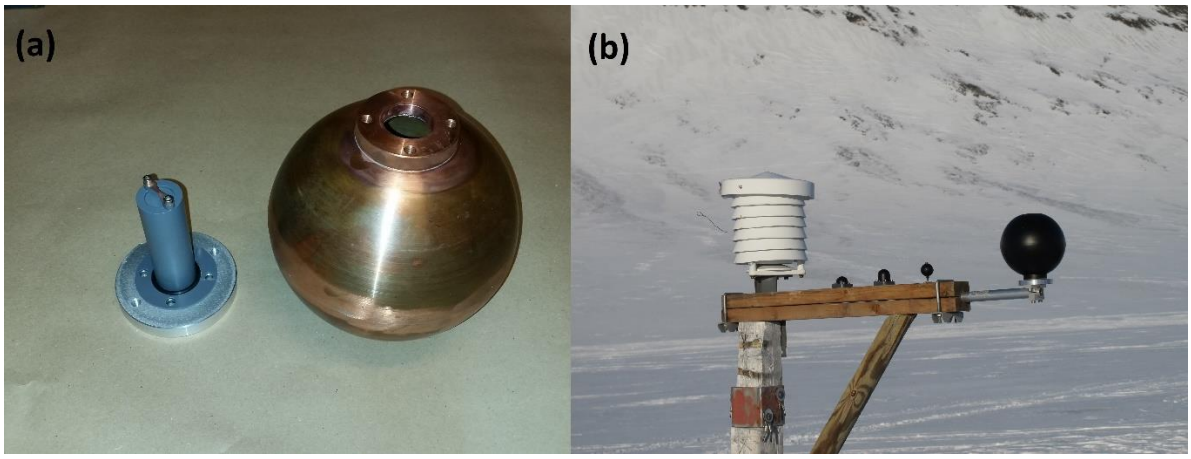

Figure S8. Construction and placement of black bulb thermistor in the study site. (a) Copper globe prior to painting. (b) Black bulb mounted on-site (right). The white structure (left) is a standard air temperature device, which together with the smaller globes (middle) are part of a separate study.

Appendix 2: Additional results

2.a Individual records

Table S1. Information about individuals used in the models of heart rate in summer (July 2018) and winter (January 2019), together with body mass (BM, kg) individual mean ± standard deviation of heart rate (in beats per minute) and subcutaneous body temperature (T_{sc}, °C). '–' means that the data was not available due to logger failure or mortality events, and the individual was not used in the analyses for winter heart rate. For both sets of data, body masses were recorded in March/April 2018 and April 2019. For calf and pregnancy statuses, '0' means not lactating or not pregnant, while '1' means lactating or pregnant, depending on season.

ID	Year born	Summer data (2018)				Winter data (2019)			
		BM	Calf	Heart rate	T_{sc}	BM	Pregnancy	Heart rate	T_{sc}
G118	2011	51.8	0	92.8±10.9	36.8±0.5	57.8	1	–	–
G140	2011	53.5	1[a]	94.6±10.3	36.2±1.1	61.3	1	36.1±12.5	33.8±2.2
G141	2011	49.5	0	89.3±9.5	36.6±0.9	52.3	1	–	–
G152	2011	47.3	1[a]	101.5±9.4	35.8±1.2	46.3	1	38.8±10.8	33.9±1.9
R289	2011	46.3	1	96.8±11.9	35.9±1.4	46.8	1	33.0±10.4	32.5±1.3
R290	2011	48.8	1	105.2±9.5	36.4±1.0	42.8	0	37.5±14.3	36.6±0.7
R297[b]	2012	47.3	0	103.8±10.0	36.0±0.9	–	–	–	–
R310	2012	50.3	0	101.7±10.3	36.3±1.1	48.3	1	–	–
R312	2012	56.3	0	99.6±13.1	36.7±0.9	55.8	1	–	–
R320	2012	46.3	1	103.7±14.7	36.8±0.8	44.8	1	40.7±20.8	35.3±1.3
W125	2010	60.0	1[a]	96.3±12.1	36.4±1.3	54.3	1	–	–
W127	2010	50.3	1	96.4±8.9	36.7±0.8	45.3	0	–	–
Y134	2013	58.8	1[a]	104.6±10.6	36.5±1.2	45.3	0	35.9±16.7	36.2±0.9
Y136	2013	45.3	1	105.0±8.4	35.5±1.9	54.3	1	37.7±7.9	31.6±4.1
Y137	2013	45.3	0	98.0±11.9	35.5±1.3	56.3	1	38.5±14.2	34.8±1.0
Y159	2013	49.3	1[a]	94.8±12.1	36.5±1.3	55.8	1	–	–
Y167	2013	52.8	1[a]	108.2±11.8	36.8±1.1	49.3	1	–	–
Y175	2013	57.0	1[a]	112.9±8.7	35.8±1.2	43.8	1	35.3±7.5	35.8±1.0
Y205	2013	53.1	1[a]	106.7±9.8	36.2±1.1	50.8	1	–	–

[a]Calf at heel inferred from pregnancy status in April and activity pattern in early July. [b]Died in March 2019, prior to scheduled body mass and pregnancy status assessment.

Table S2. Heart rate (beats per minute; bpm), subcutaneous body temperature (T_{sc}), percentage activity and environmental temperature (T_e) recorded in winter (January, N = 9) and in summer (July, N = 19). First presented are means ± standard deviation (SD) across all individuals, second for reproductive females only (lactating in summer/pregnant in winter), third for non-reproductive females only (not lactating in summer/not pregnant in winter) and finally the range (min, max) of individual means. Percent of time spent in activity was calculated as the proportion of all 5-min activity records classified as "resting" and those classified as "active". Since activity % is based on a binomial distribution (0, 1), SD was not calculated.

	Mean ± SD			**Range individual means**
	All individuals	**Reproductive**	**Non-reproductive**	
Heart rate (bpm)				
Winter				
Resting	33.7 ± 6.5	34.1 ± 5.6	32.6 ± 8.9	31.7, 35.3
Active	44.0 ± 18.4	43.8 ± 17.5	44.4 ± 20.8	36.7, 50.2
Summer				
Resting	93.0 ± 10.7	94.5 ± 10.8	90.6 ± 11.7	83.5, 108.3
Active	102.8 ± 11.3	104.0 ± 11.1	99.7 ± 11.7	91.8, 114.9
T_{sc} (°C)				
Winter				
Resting	34.1 ± 2.9	33.2 ± 3.0	36.4 ± 0.9	30.5, 36.7
Active	35.5 ± 1.2	35.1 ± 1.3	36.5 ± 0.4	34.3, 36.6
Summer				
Resting	36.2 ± 1.7	36.2 ± 1.9	36.4 ± 1.2	34.8, 37.5
Active	36.2 ± 1.0	36.2 ± 1.0	36.3 ± 1.0	35.1, 37.1
Activity %				
Winter	44	45	41	19, 49
Summer	65	67	61	42, 81
T_e (°C)				
Winter	−11.8 ± 6.5			
Summer	8.9 ± 3.7			

2.b Model selection results

Table S3. Model selection results using linear mixed-effects model with resting summer heart rate as the response variable, individual as random effect and an AR1 structure to account for within-individual temporal autocorrelation. Presented is the model structure, the likelihood ratio value (L. ratio), change in degrees of freedom (ΔDF) between original and reduced models, as well as the P-value indicating the significance level of the given change in model fit. The top model (in bold) is the one presented in the main results. Here, and in the following tables S4-S6, the abbreviated parameters refer to: t – time (in days), BM – body mass, ID- individuals, RS – reproductive status (lactation in summer, pregnancy in winter), T_e – environmental temperature and T_{sc} – subcutaneous body temperature.

#	Model parameters	L. ratio	ΔDF	P
4.	**$t + t^2 + Age + RS + T_e + T_{sc} + Age*T_{sc} + RS*T_{sc} + (1\|ID)$**	1.739	1	0.872
3.	$t + t^2 + Age + BM + RS + T_e + T_{sc} + Age*T_{sc} + RS*T_{sc} + (1\|ID)$	0.880	1	0.348
2.	$t + t^2 + Age + BM + RS + T_e + T_{sc} + Age*T_{sc} + RS*T_{sc} + T_e*T_{sc} + (1\|ID)$	0.117	1	0.732
1.	$t + t^2 + Age + BM + RS + T_e + T_{sc} + Age*T_{sc} + BM*T_{sc} + RS*T_{sc} + T_e*T_{sc} + (1\|ID)$			

Table S4. Model selection results using linear mixed-effects model with summer heart rate during activity as the response variable, individual as random effect and an AR1 structure to account for within-individual temporal autocorrelation. Presented is the model structure, the likelihood ratio value (L. ratio), change in degrees of freedom (ΔDF) between original and reduced models, as well as the P-value indicating the significance level of the given change in model fit. The top model (in bold) is the one presented in the main results.

#	Model parameters	L. ratio	ΔDF	P
4.	**$t + t^2 + Act + Age + BM + RS + T_e + T_{sc} + Act*T_{sc} + Act*BM + Age*T_{sc} + RS*T_{sc} + (1\|ID)$**	3.440	1	0.064
3.	$t + t^2 + Act + Age + BM + RS + T_e + T_{sc} + Act*T_a + Act*T_{sc} + Act*BM + Age*T_{sc} + RS*T_{sc} + (1\|ID)$	2.343	1	0.126
2.	$t + t^2 + Act + Age + BM + RS + T_e + T_{sc} + Act*T_e + Act*T_{sc} + Act*BM + Age*T_{sc} + BM*T_{sc} + RS*T_{sc} + (1\|ID)$	0.149	1	0.699
1.	$t + t^2 + Act + Age + BM + RS + T_e + T_{sc} + Act*T_a + Act*T_{sc} + Act*BM + Age*T_{sc} + BM*T_{sc} + RS*T_{sc} + T_e*T_{sc} + (1\|ID)$			

Table S5. Model selection results using linear mixed-effects models with resting winter heart rate as the response variable, individual as random effect and an AR1 structure to account for within-individual temporal autocorrelation. Presented is the model structure, the likelihood ratio value (L. ratio), change in degrees of freedom (ΔDF) between original and reduced models, as well as the P-value indicating the significance level of the given change in model fit. The top model (in bold) is the one presented in the main results.

#	Model parameters	L. ratio	ΔDF	P
5.	**t + Age + RS + T_e + T_{sc} + Age*T_{sc} + (1|ID)**	0.031	1	0.860
4.	t + Age + BM + RS + T_e + T_{sc} + Age*T_{sc} + (1|ID)	2.652	1	0.103
3.	t + Age + BM + RS + T_e + T_{sc} + Age*T_{sc} + T_e*T_{sc} + (1|ID)	0.444	1	0.505
2.	t + Age + BM + RS + T_e + T_{sc} + Age*T_{sc} + BM*T_{sc} + T_e*T_{sc} + (1|ID)	0.005	1	0.944
1.	t + Age + BM + RS + T_e + T_{sc} + Age*T_{sc} + BM*T_{sc} + RS*T_{sc} + T_e*T_{sc} + (1|ID)			

Table S6. Model selection results using linear mixed-effects models with winter heart rate during activity as the response variable, individual as random effect and an AR1 structure to account for within-individual temporal autocorrelation. Presented is the model structure, the likelihood ratio value (L. ratio), change in degrees of freedom (ΔDF) between original and reduced models, as well as the P-value indicating the significance level of the given change in model fit. The top model (in bold) is the one presented in the main results.

#	Model parameters	L. ratio	ΔDF	P
3.	**t + Act + Age + BM +RS + T_e + T_{sc} + Act*T_{sc} + Act*BM + Age*T_{sc} + BM*T_{sc} + RS*T_{sc}+ (1|ID)**	1.439	1	0.230
2.	t + Act + Age + BM +RS + T_e + T_{sc} + Act*T_{sc} + Act*BM + Age*T_{sc} + BM*T_{sc} + RS*T_{sc}+ T_e*T_{sc} + (1|ID)	0.573	1	0.230
1.	t + Act + Age + BM +RS + T_e + T_{sc} + Act*T_e + Act*T_{sc} + Act*BM + Age*T_{sc} + BM*T_{sc} + RS*T_{sc}+ T_e*T_{sc} + (1|ID)			

2.c Additional results (figures)

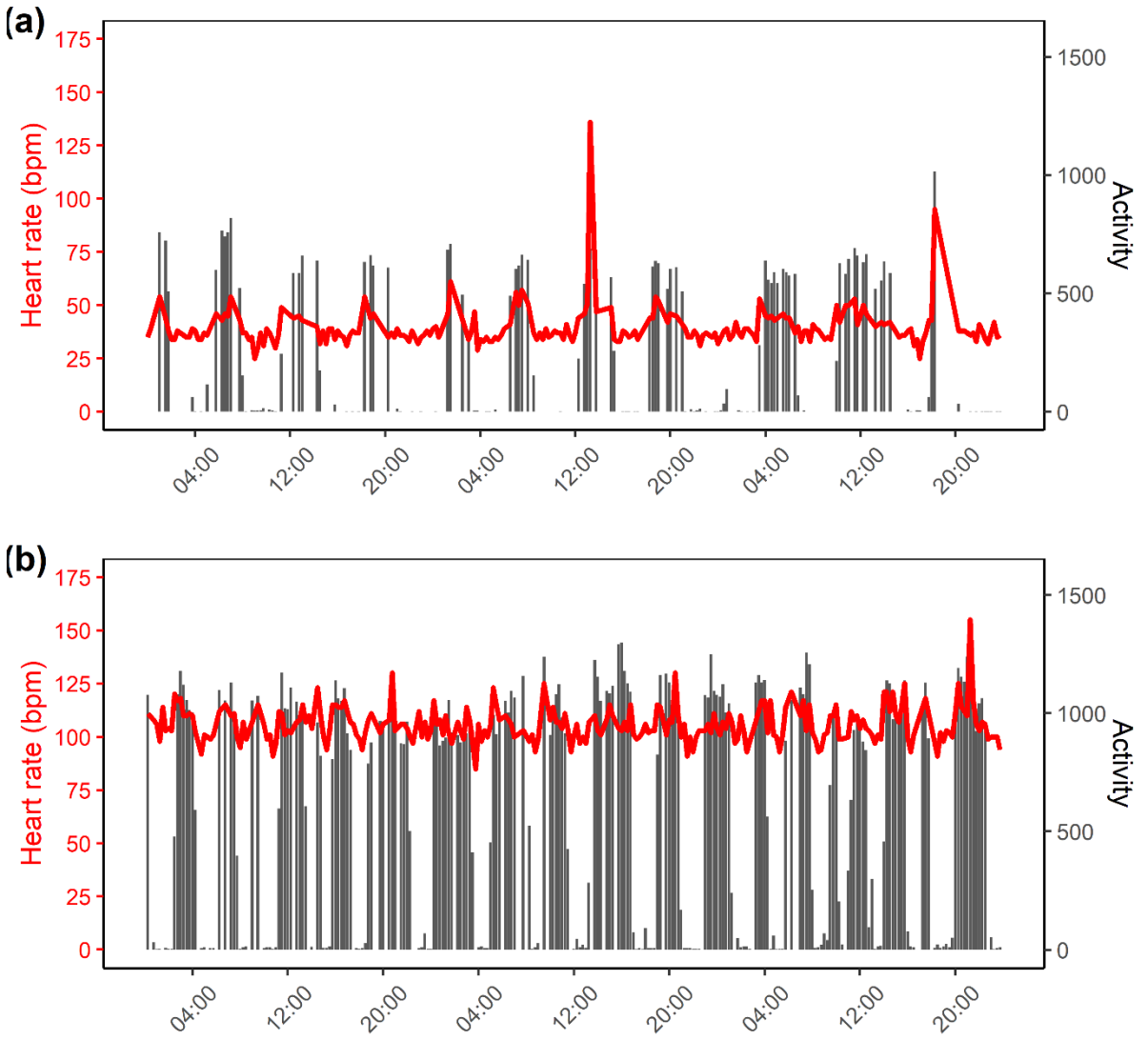

Figure S9. 15-min recordings of heart rate (left y-axis) and activity (right y-axis, ranging from 0 to 1530, where 0 represents no activity and 1530 maximum activity) spanning over 72 hours in a Svalbard reindeer female, in **(a)** January (11^{th} – 13^{th}) and **(b)** July (11^{th} – 13^{th}). The red lines show the heart rate (beats per minute, bpm) while the grey bars represent activity levels as a sum of acceleration in the X and Y directions every 15 minutes (details described in methods).

When generating predicted heart rates presented in figures and results, we expanded data sets starting at the lowest 1% to the upper 99% of the distribution of the predictor variable of interest, while other variables were fixed at mean values (this being 0 when scaled), except in interactions where the interacting variable was fixed at 3 categories, representing the 0.15, 0.5 and 0.85 quantiles of their distribution. Confidence intervals (95%) were generated by multiplying the standard error of the estimates by 1.96.

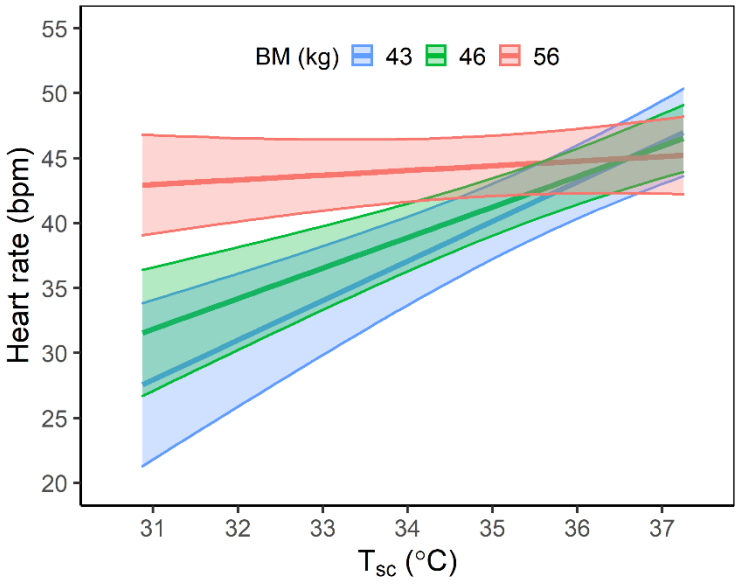

Figure S10. Predicted active heart rate (± 95% confidence intervals) of Svalbard reindeer females plotted against subcutaneous body temperature (T_{sc}, °C) during winter (N = 9, R^2 = 0.03; table 1) showing the interaction with April body mass (BM, kg). Body mass was fitted as a continuous variable, and the values here represent the 0.15, 0.5 and 0.85 quantiles from the distribution of body masses.

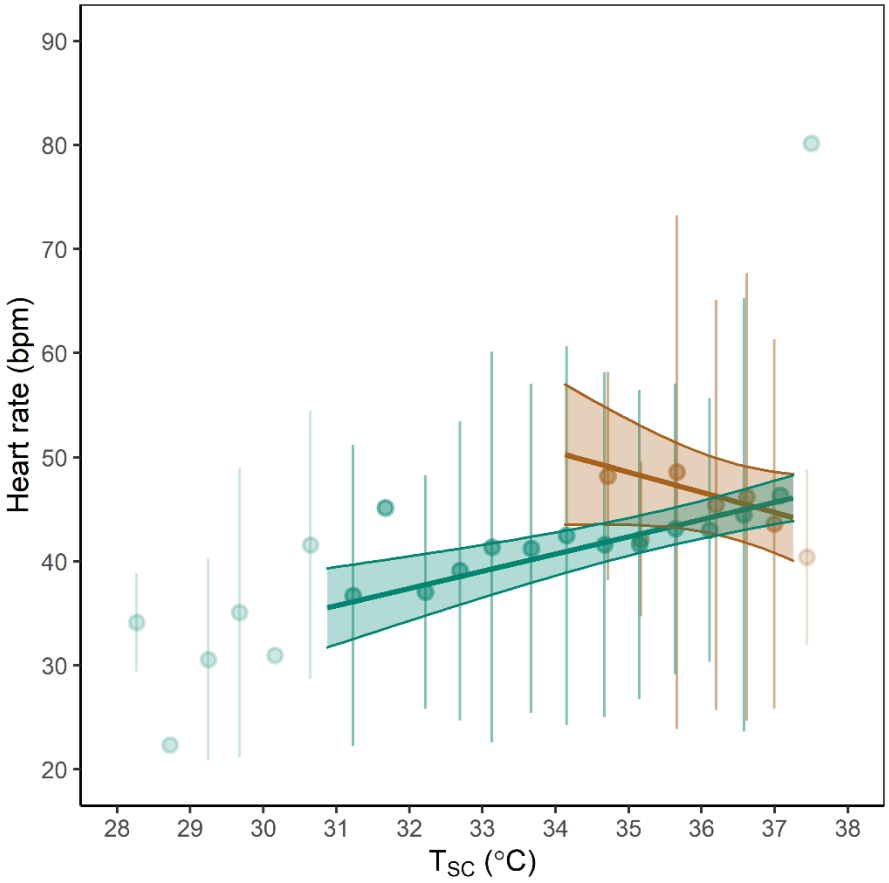

Figure S11. Predicted active heart rate (± 95% confidence intervals) of Svalbard reindeer females in winter, plotted against subcutaneous body temperature (T_{sc}, °C) in interaction with reproductive status (green = pregnant, brown = not pregnant). The solid lines represent predicted response in each activity state (see table 1 for details) and shaded areas represent 95% confidence intervals (CI) of the model predictions. Points and their error bars represent mean ± standard deviation of heart rate adjusted for the other model predictors (table 1). Points that fall outside the predicted range are values below the lower 0.01 or above the upper 0.99 quantiles of the T_{sc} distribution for each reproductive group.

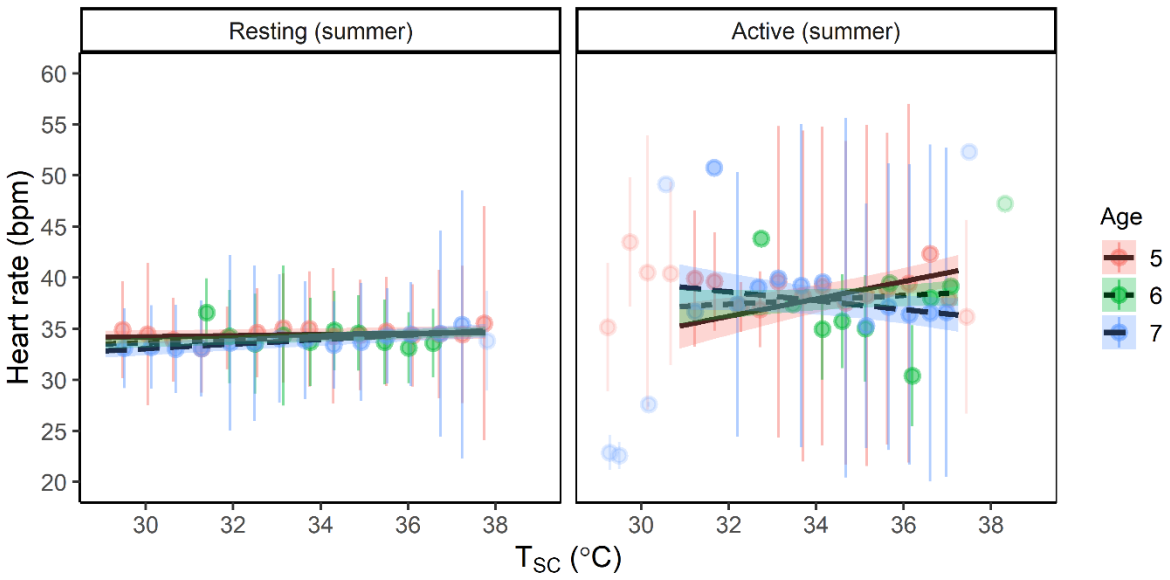

Figure S12. Predicted heart rate (± 95% confidence intervals) of Svalbard reindeer females winter, plotted against subcutaneous body temperature (T_{sc}, °C) in interaction with age (in years) during resting (left panel) and while active (right panel). Points and their error bars represent mean ± standard deviation adjusted for the other model variables (table 1). The lightly shaded points are values below the lower 0.01 or above the upper 0.99 quantiles of T_{sc}, i.e. representing less than 2% of the data.

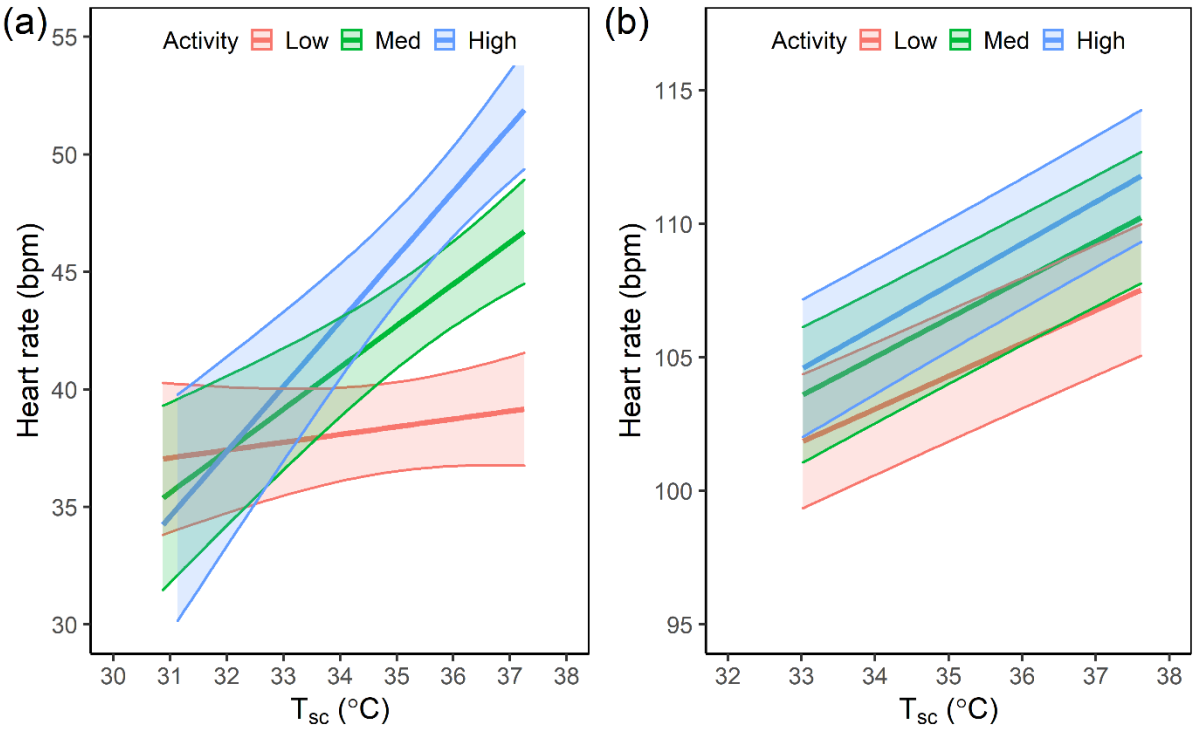

Figure S13. Predicted active heart rate (± 95% confidence intervals) of Svalbard reindeer females in winter, plotted against subcutaneous body temperature (T_{sc}, °C) in interaction with activity, grouped into "low", "medium" and "high" intensity based on the 0.15, 0.5 and 0.85 quantiles of the distribution of activity in each season: (a) winter (N = 9), and (b) summer (N = 19).

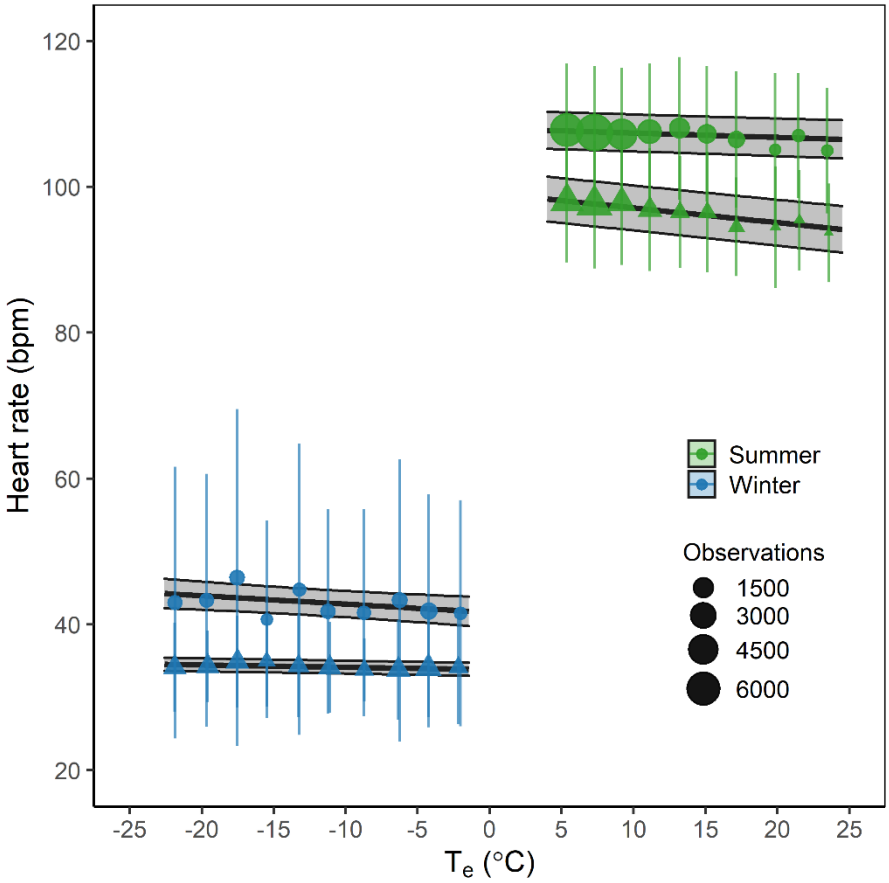

Figure S14. Predicted heart rate (± 95% confidence intervals) of Svalbard reindeer females, plotted against environmental temperature (T_e) (data binned with increments of 2.5°C) in summer (green) and winter (blue). The solid lines represent heart rate predicted from linear mixed-effects models in each season (table 1) and shaded areas represent 95% confidence intervals of the model predictions. Points and their error bars represent mean ± standard deviation adjusted for the other model variables (table 1). The size of each point represents the number of unique recordings per temperature increment.

References for supplementary material

1. Bjørkvoll E, Pedersen B, Hytteborn H, Jónsdóttir IS, Langvatn R. 2009 Seasonal and Interannual Dietary Variation During Winter in Female Svalbard Reindeer (*Rangifer Tarandus Platyrhynchus*). *Arctic, Antarct. Alp. Res.* **41**, 88–96. (doi:10.1657/1523-0430-41.1.88)
2. Van Der Wal R, Stien A. 2014 High-arctic plants like it hot: A long-term investigation of between-year variability in plant biomass. *Ecology* **95**, 3414–3427. (doi:10.1890/14-0533.1)
3. Le Moullec M, Pedersen ÅØ, Stien A, Rosvold J, Hansen BB. 2019 A century of conservation: The ongoing recovery of Svalbard reindeer. *J. Wildl. Manage.* **83**, 1676–1686. (doi:10.1002/jwmg.21761)
4. Hansen BB, Aanes R, Sæther BE. 2010 Feeding-crater selection by high-arctic reindeer facing ice-blocked pastures. *Can. J. Zool.* **88**, 170–177. (doi:10.1139/Z09-130)
5. StarOddi. 2020 DST centi-HRT Heart Rate and Temperature Logger [Online]. See https://www.star-oddi.com/products/data-loggers/animal-heart-rate-activity-logger.
6. Krop-Benesch A, Berger A, Streich J, Scheibe K. 2011 Activity Pattern - User's Manual VECTRONIC Aerospace.
7. Lyftingsmo E. 2016 Combining GPS activity measurements and real-time video recordings to quantify the activity budget of wild reindeer (Rangifer tarandus). Norwegian University of Life Sciences.
8. Reimers E. 1979 Activity pattern: The major determinant for growth and fattening in Rangifer? In *Reindeer/Caribou Symposium II Norway* (eds E Reimers, E Gaare, S Skjenneberg), pp. 466–474. Direktoratet for Vilt og Ferskvannsfisk.